An exact method to obtain effective electrostatic interactions from computer simulations: The case of effective charge amplification

P. González-Mozuelos, G. I. Guerrero-García, and M. Olvera de la Cruz

Additional information on J. Chem. Phys.

An exact method to obtain effective electrostatic interactions from computer simulations: The case of effective charge amplification

P. González-Mozuelos,[1,2] G. I. Guerrero-García,[1] and M. Olvera de la Cruz[1,3,a]

[1]*Department of Materials Science and Engineering, Northwestern University, Evanston, Illinois 60208, USA*
[2]*Departamento de Física, Cinvestav del I. P. N., Av. Instituto Politécnico Nacional 2508, Distrito Federal, C. P. 07360, Mexico*
[3]*Department of Chemistry, Northwestern University, Evanston, Illinois 60208, USA*

We discuss here an exact method to determine the parameters regulating the screened Coulomb interactions among spherical macroions immersed in a simple electrolyte. This approach provides rigorous definitions for the corresponding screening length, effective permittivity, and renormalized charges, and can be employed for precise and reliable calculations of these parameters within any scheme. In particular, we introduce a simple procedure for extracting this information from computer simulations. The viability of this approach is demonstrated by applying it to a three-component model system which includes anionic nanoparticles and monovalent cations and anions. The mean forces between nanoparticles are determined directly from simulations with two macroions, plus small ions, inside a single cell with periodic boundary conditions. The values of the parameters of interest, on the other hand, are gathered from two separate sets of computer simulations: one set provides information about the short-range correlations among the small ions, which in turn determine the screening length and effective permittivity; the second set supplies the short-range components of the ionic distribution around one isolated macroion, which also determine its renormalized charge. The method presented here thus avoids the uncertain fitting of these parameters from the asymptotic tail of the mean force and allows us to investigate in detail this connection between the renormalized charge of the macroion and the short-range (virtual) part of the ionic cloud surrounding it. Using the standard prescription to extract an effective charge from the corresponding renormalized value, we then proceed to clarify the mechanisms behind the possibility of effective charge amplification (i.e., an effective charge larger than the bare macroion charge). Complementarily, we report results for the corresponding bridge functions too. © *2013 AIP Publishing LLC*. [http://dx.doi.org/10.1063/1.4817776]

I. INTRODUCTION

Charged colloids in aqueous solutions are of paramount importance in a wide range of technological, industrial, biological, and physicochemical applications. Two well established experimental techniques applied to the study of colloidal suspensions, light scattering,[1–7] and optical microscopy,[8–17] have provided a wealth of information about the static structure and dynamic properties of the suspended macroions. An important characteristic of these experimental techniques is that the length scales probed by them, of the order of 10 nm–5000 nm, are much larger than the typical size of the remaining components in the system, namely, the small ions and solvent molecules in the suspension. The information obtained by these means is thus mostly related to the correlations among the colloidal particles (macroions), and anything corresponding to the other components of the suspension has to be inferred indirectly. This situation has also been mirrored in the corresponding theoretical research, where many endeavors have been directed to the development of models in which only the observable macroparticles are explicitly taken

into account. The main point of these models is the description of the interactions among the macroparticles in terms of effective pair potentials (EPPs), which, in principle, emerge from averaging out the unobservable components. The best known model for colloidal suspensions of charged spherical particles is based on the Derjaguin-Landau-Verwey-Overbeek (DLVO) potential, basically given by a combination of hard sphere repulsion and van der Waals attraction for the short range component of the macroion-macroion interaction, plus a screened Coulomb (Yukawa) potential for the long range component of this interaction.[18,19] Historically, this model provided the first successful description of the stability of colloidal suspensions controlled by the irreversible flocculation of the suspended colloids. A stripped-down version of this model, in which the van der Waals component is neglected, has also been quite successful in the description of the two-point correlations observed in sufficiently dilute suspensions with moderately low salt concentrations.

The electrostatic component of the DLVO potential, originally obtained within the context of the linearized Poisson-Boltzmann (PB) equation, has also been rigorously derived from the primitive model level of description, which assumes that the solvent is a structureless continuum and models all the ionic species as charged hard spheres of

a)Author to whom correspondence should be addressed. Electronic mail: m-olvera@northwestern.edu

different sizes and charges, by using the Ornstein-Zernike (OZ) equation in combination with the mean spherical approximation (MSA) for the correlations among all the components in the system. The standard DLVO result is then gained by assuming the small ions to be point-like, thus making the MSA closure equivalent to the Debye-Hückel approximation for the correlations among these small ions, while keeping the size of the macroions finite but taking the limit of infinite macroion dilution.[20] Under these conditions, it is still possible to consider polydispersity in colloid size and charge.[19] This line of inquire (about effective interactions among macroions) has been extended to less restrictive conditions, still within the solvent as a structureless background (McMillan-Mayer) level of description, by considering non-linear correlations between macroions and small ions, finite macroion concentrations, finite small ion sizes, and spontaneous charge regulation.[20–55]

A central conclusion from these theoretical studies has been the confirmation of the screened Coulomb model for the long-range effective interactions among macroions, at least for sufficiently dilute supporting electrolytes. The main features of this model are its screening length, determined mainly by the electrolyte concentration, and the renormalized charges, regulated mostly by the short-range distributions of small ions around the macroions. A rather standard prescription,[23,33,38,46,52] employed in many cases, defines an effective macroion charge by equating the obtained renormalized charge to the corresponding DLVO formula. It is also often assumed that the corresponding screening length is identical to the Debye length, which is true only within a mean-field approach for the correlations among the small ions in an infinitely extended system.[26,32,36,38,40,43,52] Trizac and collaborators,[46] however, have shown that even within this level of approximation this is not necessarily true when considering (finite) Wigner-Seitz cells, besides providing useful analytical relationships that facilitate the determination of the effective charges. On the other hand, the divergence between the real screening length and the Debye value has been confirmed by computer simulation studies.[39,41,50,55] Moreover, even the additivity of the effective charges has been called into question by this type of studies,[50] prompting the demand for a deeper understanding of these issues.

A general and rigorous theoretical framework for the definition of the parameters involved in the screened Coulomb potential, based on the synthesis of the exact techniques from the dressed ion theory developed by Kjellander and Mitchell[56,57] with the precise definition of effective direct correlation functions,[25–27] already exists.[36,43] This scheme shows explicitly how the relevant parameters (e.g., screening length and renormalized charges) are connected to the short-range components of the correlations among the diverse ionic species in the suspension, while clearly distinguishing between its observable and unobservable constituents; therefore, any *ad hoc* assumptions about the nature of these parameters are avoided. The main purpose of the present work is to provide a detailed description of a simple and direct approach, based on the ideas first proposed by Ulander and Kjellander,[58] that allows the implementation of this conceptual framework to computer simulation studies of colloidal suspensions. This

method thus circumvents the shortcomings present in most theoretical schemes, which provide only approximated answers, while reducing the uncertainty involved in fitting the simulation data to the model potential. Moreover, such approach should help to elucidate some outstanding questions about the foundations of the screened Coulomb potential, and the limits of its applicability. The general scheme described here is tested by considering a model three-component system, constituted by anionic nanoparticles plus monovalent anions and cations. Among other interesting results, it is found that, under suitable conditions, the macroion effective charge may become larger in magnitude than the corresponding bare charge. The impact of this and other effects on the overall stability of the colloidal suspension is discussed elsewhere.[63] Here, we present an extended analysis of mechanisms underlying this charge amplification, based on the examination of the short-range (virtual) ionic distributions dressing each macroion. Such analysis substantiates the argument that the presence of large counterions allows the adsorption of the smaller coions to the macroion surface, thus inducing the inefficient electrostatic shielding (nonlinear screening) that augments its effective charge.

In Sec. II, we describe the exact procedure for obtaining the effective direct correlation functions, which emerge after averaging out the unobservable species (i.e., the supporting electrolyte), and the definition of the effective pair potentials in terms of these correlation functions. Section III provides a brief description of the results gained by applying the rigorous dressed ion theory approach to these effective direct correlation functions, and how these results in turn establish the definitions of the parameters governing the long-range interactions among the macroions: the effective permittivity and screening length, emerging mostly from the supporting electrolyte, and the renormalized charges of the observable macroions, determined by the short-range correlations between them and the small ions. Section IV gives an account of the model system and the computer simulation approach used to calculate the mean forces, as well as the general scheme employed to produce the short-range correlations needed for the determination of the screened Coulomb parameters. The ensuing results are then presented in Sec. V, with a discussion of the nature of the virtual charge distributions that induce the renormalized charges and the properties of the corresponding bridge functions. Concluding remarks are provided in Sec. VI.

II. EFFECTIVE INTERACTIONS IN MULTICOMPONENT SYSTEMS

The description of the microscopic structure of an uniform multicomponent fluid with M species of spherical particles entails the determination of the full set of $M(M + 1)/2$ independent radial distribution functions $g_{ij}(r) \equiv h_{ij}(r) + 1$, where $h_{ij}(r)$ is the two-point total correlation function between a particle of species i and a particle of species j separated by a distance r, taking into account that $h_{ij}(r) = h_{ji}(r)$. Standard theoretical approaches for the determination of these correlation functions make use of the set of OZ equations, which in

Fourier space take the form

$$\tilde{h}_{ij}(k) = \tilde{c}_{ij}(k) + \sum_{p=1}^{M} \tilde{c}_{ip}(k) \, \rho_p \, \tilde{h}_{pj}(k) \qquad (1)$$

for $i, j = 1, 2, \ldots, M$, where ρ_p is the number density of particles of species p in the system. These equations may simply be regarded as the definition of the direct correlation functions $c_{ij}(r)$ in terms of the corresponding total correlation functions, and their Fourier transformed versions are indeed related to the corresponding real space functions by the usual prescription,

$$\tilde{\chi}(k) \equiv 4\pi \int_0^\infty dr \, r^2 \, j_0(kr) \, \chi(r), \qquad (2)$$

where $j_0(x) \equiv \sin(x)/x$ is the spherical Bessel function of order zero. Assuming that all the interactions are pairwise additive, the OZ equations are then complemented by the closure relations

$$c_{ij}(r) = -\beta u_{ij}(r) + h_{ij}(r) - \ln(1 + h_{ij}(r)) + b_{ij}(r) \qquad (3)$$

for $i, j = 1, \ldots, M$, where $u_{ij}(r)$ is the pair potential between a particle of species i and one of species j, $\beta \equiv (k_B T)^{-1}$, k_B is the Boltzmann constant, and T is the temperature of the system. Equation (3) can also be interpreted as the definition of the bridge functions $b_{ij}(r)$.

For many situations of interest, however, dealing with the full set of $M(M + 1)/2$ independent correlation functions is excessive or impractical, particularly in light of the fact that usually only a subset of the components is directly observed in a given experimental setup. From the theoretical side, this partial knowledge of the structure can be interpreted in terms of the EPPs, which account for the measured correlations and are mediated by the unobservable components. The standard approach[36] for the determination of these EPPs starts by rewriting Eq. (1) in the matrix form

$$\mathbf{H} = \mathbf{C} + \mathbf{C}\,\mathbf{R}\,\mathbf{H}, \qquad (4)$$

where $[\mathbf{R}]_{ij} = \rho_i \delta_{ij}$, $[\mathbf{H}]_{ij} = \tilde{h}_{ij}(k)$, and $[\mathbf{C}]_{ij} = \tilde{c}_{ij}(k)$. Thus, for all these matrices $\mathbf{X}^T = \mathbf{X}$, where the superscript T means transpose, and $\mathbf{X}$ stands for $\mathbf{R}$, $\mathbf{H}$, or $\mathbf{C}$. If $m < M$ is the number of observable species in the system, then each one of the matrices in the previous equation can be partitioned in accordance with this distinction between observable and unobservable species,

$$\mathbf{X} = \begin{pmatrix} \mathbf{X}_{OO} & \mathbf{X}_{OB} \\ \mathbf{X}_{BO} & \mathbf{X}_{BB} \end{pmatrix}, \qquad (5)$$

where the subscript O corresponds to the subset of m observable components, whereas the subscript B corresponds to the subset of $M - m$ background (unobservable) components. The density matrix $\mathbf{R}$ is diagonal, and therefore $\mathbf{R}_{OB} = \mathbf{R}_{BO}^T = \mathbf{0}$, where $\mathbf{0}$ is the appropriate null matrix. Also for simplicity, we define $\mathbf{R}_O \equiv \mathbf{R}_{OO}$ and $\mathbf{R}_B \equiv \mathbf{R}_{BB}$. This matrix partition can then be used to rewrite Eq. (4) as a set of four interconnected matrix equations, which upon recombination yield the contracted OZ equation

$$\mathbf{H}_{OO} = \mathbf{C}_{OO}^{\text{eff}} + \mathbf{C}_{OO}^{\text{eff}} \, \mathbf{R}_O \, \mathbf{H}_{OO}, \qquad (6)$$

where

$$\mathbf{C}_{OO}^{\text{eff}} = \mathbf{C}_{OO} + \mathbf{C}_{OB} \left(\mathbf{R}_B^{-1} - \mathbf{C}_{BB} \right)^{-1} \mathbf{C}_{BO} \qquad (7)$$

is the $m \times m$ matrix of effective direct correlation functions that reproduce the observable total correlation functions.

In the final step, the EPPs among the observable components, $u_{ij}^{\text{eff}}(r)$, are defined by the equivalent of Eq. (3),

$$c_{ij}^{\text{eff}}(r) = -\beta u_{ij}^{\text{eff}}(r) + h_{ij}(r) - \ln(1 + h_{ij}(r)) + b_{ij}(r; \{u^{\text{eff}}\}), \qquad (8)$$

for $i, j = 1, \ldots, m$, where we have indicated that the corresponding bridge functions should be evaluated as functionals of the EPPs. A perhaps more useful relation is obtained by combining this last definition with the original bridge equation (3) to yield the expression

$$\beta u_{ij}^{\text{eff}}(r) = \beta u_{ij}(r) + c_{ij}(r) - c_{ij}^{\text{eff}}(r) + b_{ij}(r; \{u^{\text{eff}}\}) - b_{ij}(r; \{u\}), \qquad (9)$$

which links more directly these EPPs to the corresponding bare pair potentials. In the contracted description just described, the unobservable particles have been removed, leaving us with an effective system where the interactions among the remaining particles are given by the emerging EPPs. It should be mentioned that, in general, no exact solution may exist for these EPPs, and approximate expressions for $b_{ij}(r; \{u\})$ must be unavoidable in most instances. Furthermore, the EPPs defined in this way provide only the correct two-body distribution functions and it is not to be expected that higher-order correlations would be accurately accounted by them. Nevertheless, in the limit of infinite dilution of observable particles ($\mathbf{R}_O = \mathbf{0}$) the EPPs become identical to the potentials of mean force (PMFs) among these observable particles, which are defined as $\beta w_{ij}(r) \equiv -\ln(1 + h_{ij}(r))$, thus connecting the present approach with other commonly used techniques.

Even though the EPPs defined by Eq. (8) may not exist, the effective direct correlation functions introduced in Eq. (6) are always well characterized. Let us consider the internal potential energy of our system as a function of the positions of the observable and background components: $\hat{V}(\{\mathbf{r}\}_O, \{\mathbf{r}\}_B)$. The effective potential energy of the observable components is then attained by integrating out the unobservable particles,

$$\beta \hat{V}_O^{\text{eff}}(\{\mathbf{r}\}_O) = -\ln\left[\prod_{\gamma \in B} \left(\Lambda_\gamma^{3N_\gamma} N_\gamma! \right)^{-1} \right.$$
$$\left. \times \int d\{\mathbf{r}\}_B \, \exp(-\beta \hat{V}(\{\mathbf{r}\}_O, \{\mathbf{r}\}_B)) \right], \quad (10)$$

where Λ_γ and N_γ are, respectively, the thermal de Broglie wavelength and number of particles of species γ. Therefore, the set of functions $c_{ij}^{\text{eff}}(r)$ are given, in the thermodynamic limit, by the second functional derivative with respect to the corresponding local densities of the intrinsic excess free energy pertaining to this effective potential energy (see Appendix A). In general, $\hat{V}_O^{\text{eff}}(\{\mathbf{r}\}_O)$ is not pairwise additive, even when $\hat{V}(\{\mathbf{r}\}_O, \{\mathbf{r}\}_B)$ is so. Nonetheless, as shown in Sec. III, for the effective electrostatic interactions such pairwise additivity is invariably guaranteed.

III. DRESSED ION THEORY FOR THE EFFECTIVE PAIR POTENTIALS

The definitions of Sec. II can be profitably applied to charged fluid systems in which the electrostatic interactions play a central role in the determination of their microscopic and thermodynamic properties.[36] Let us start by considering the general case in which there is a spherical charge distribution $z_i(r)$ (in units of e) associated to each particle of species i. Hence, the Fourier transformed pair potential between a particle of species i and one of species j takes the form

$$\beta \tilde{u}_{ij}(k) = \beta \tilde{u}_{ij}^s(k) + \tilde{z}_i(k) \ell_b \tilde{v}(k) \tilde{z}_j(k), \qquad (11)$$

where $u_{ij}^s(r)$ is the short-range part of the interaction, $\ell_b \equiv e^2/4\pi \varepsilon_r \varepsilon_0 k_B T$ is the Bjerrum length of the system of interest, e is the proton charge, ε_0 is the vacuum permittivity, and ε_r is the dielectric constant of the background. Although it is usually assumed that the electrostatic potential is of the form $v(r) = r^{-1}$, for the sake of generality it will be assumed here only that it takes this form in the asymptotic regime, so $\lim_{r \to \infty} r \, v(r) = 1$. In this case, we have that

$$\tilde{v}(k) = \frac{4\pi \, f(k)}{k^2}, \qquad (12)$$

where the function $f(k)$ is analytic, even, and such that $f(0) = 1$ and $\lim_{k \to \infty} |f(k)| < \infty$. From Eq. (2), and using the fact that $j_0(0) = 1$, it is clear that $q_i \equiv \tilde{z}_i(0)$ is the total charge (in units of e) associated with a particle of species i. Furthermore, the kind of uniform charged system considered here must fulfill the global electroneutrality condition $\sum_{i=1}^{M} \rho_i q_i = 0$ to be thermodynamically stable.

From Eqs. (3) and (11) then follows that the functions $\tilde{c}_{ij}(k)$ take the form

$$\tilde{c}_{ij}(k) = \tilde{c}_{ij}^s(k) - \tilde{z}_i(k) \ell_b \tilde{v}(k) \tilde{z}_j(k) \qquad (13)$$

for $i, j = 1, 2, \ldots, M$, where the functions $\tilde{c}_{ij}^s(k)$ are the corresponding short-range components of the direct correlation functions. In matrix notation, this reads like

$$\mathbf{C} = \mathbf{C}^s - \ell_b \tilde{v}(k) \mathbf{Z} \mathbf{Z}^T, \qquad (14)$$

where the column vector $\mathbf{Z}$ has the components $[\mathbf{Z}]_i = \tilde{z}_i(k)$. Using the partition $\mathbf{Z}^T = (\mathbf{Z}_O^T, \mathbf{Z}_B^T)$ when introducing this last result into Eq. (7), and following the methods first developed by Kjellander and Mitchell,[56,57] one arrives to the desired set of results,[36,43]

$$\mathbf{C}_{OO}^{\text{eff}} = \mathbf{C}_{OO}^s + \mathbf{C}_{OB}^s \mathbf{W}_B \mathbf{C}_{BO}^s - \ell_b \tilde{v}^{(R)}(k) \mathbf{Z}_O^{(R)} \mathbf{Z}_O^{(R)T}, \qquad (15)$$

where we have introduced the auxiliary matrix

$$\mathbf{W}_B \equiv \left(\mathbf{R}_B^{-1} - \mathbf{C}_{BB}^s \right)^{-1}, \qquad (16)$$

the renormalized charge distributions given by

$$\mathbf{Z}_O^{(R)} \equiv \mathbf{Z}_O + \mathbf{C}_{OB}^s \mathbf{W}_B \mathbf{Z}_B, \qquad (17)$$

and the renormalized electrostatic potential $\tilde{v}^{(R)}(k)$, related to the bare electrostatic potential by the recursive relation

$$\tilde{v}^{(R)}(k) = \tilde{v}(k) - \tilde{v}(k) \frac{\kappa_B^2(k)}{4\pi} \tilde{v}^{(R)}(k), \qquad (18)$$

with the screening function given by

$$\kappa_B^2(k) \equiv 4\pi \ell_b \mathbf{Z}_B^T \mathbf{W}_B \mathbf{Z}_B. \qquad (19)$$

From the combination of Eqs. (12) and (18) follows that the renormalized electrostatic potential takes the form

$$\tilde{v}^{(R)}(k) = \frac{4\pi \, f(k)}{k^2 + f(k) \kappa_B^2(k)}, \qquad (20)$$

and therefore its asymptotic behavior will, in general, differ from that of $\tilde{v}(k)$. Finally, Eqs. (9) and (15) then lead us to the conclusion that the EPPs in charged simple fluids are actually of the general form

$$\beta \tilde{u}_{ij}^{\text{eff}}(k) = \beta \tilde{u}_{ij}^{se}(k) + \beta \tilde{u}_{ij}^{ee}(k), \qquad (21)$$

with the effective electrostatic pair interaction given by

$$\beta \tilde{u}_{ij}^{ee}(k) = \tilde{z}_i^{(R)}(k) \ell_b \tilde{v}^{(R)}(k) \tilde{z}_j^{(R)}(k) \qquad (22)$$

for $i, j = 1, 2, \ldots, m$, where $\tilde{z}_i^{(R)}(k) = [\mathbf{Z}_O^{(R)}]_i$ and $u_{ij}^{se}(r)$ is the corresponding short-range component of this effective pair potential.

As mentioned above, even if the EPPs may not rigorously exist in general, the effective electrostatic interaction of Eq. (22) remains true in all cases. This last result follows directly from Eq. (15), which in turn depends only on the form of $c_{ij}(r)$ given in Eq. (13), and has nothing to do with the definition in Eq. (8). Therefore, for systems with charged particles the effective potential energy defined in Eq. (10) has always a pairwise additive component constituted by sums of $\beta u_{ij}^{ee}(r)$. This universality encompasses, of course, the renormalized charge distributions and electrostatic potential defined in Eqs. (17) and (18), respectively.

The main interest of these results concern their application to the determination of the asymptotic behavior of the effective interactions among macroions immersed in a simple electrolyte.[56,57] According to the residue theorem, this behavior will be determined by the poles of $\tilde{u}_{ps}^{\text{eff}}(k)$ in the upper half of the complex k-plane closest to the real axis. For sufficiently dilute solutions, the single dominant pole comes from the renormalized electrostatic potential $\tilde{v}^{(R)}(k)$ and is purely imaginary. Denoting this pole by $k = i\eta$, we then have that

$$\ell_b v^{(R)}(r) \sim \frac{\ell_b}{E^{(R)} r} \exp(-\eta r), \qquad (23)$$

where $E^{(R)}$ comes from the corresponding residue; therefore, η^{-1} plays the role of an effective screening length and $E^{(R)}$ accounts for the electric polarizability of the supporting electrolyte. Under these circumstances, one can then posit that the EPP between two spherical macroions in a polydisperse solution always takes the general form

$$\beta u_{ps}^{\text{eff}}(r) = \beta u_{ps}^*(r) + \frac{\ell_b}{E^{(R)} r} \exp(-\eta r) A_p A_s \qquad (24)$$

for $p, s = 1, 2, \ldots, m$ (p and s denote the observable components for the rest of this section), where $A_p \equiv \tilde{z}_p^{(R)}(i\eta)$ is the renormalized charge of a macroion of type p in elementary charge units and $u_{ps}^*(r)$ represents the effective short-range interaction between these macroions. In this short-range term, we are throwing in all the contributions that do not fit the asymptotic Yukawa form; that is, not only $u_{ps}^{se}(r)$, but also the

non-asymptotic contributions from $u_{ps}^{ee}(r)$ in Eq. (22). Compared to the possibility of asymptotic terms of the general form $\ell_b M_{ps} \exp(-\eta_{ps} r)/E^{(R)} r$, it is a significant conclusion from the exact dressed ion theory analysis that not only all the screening lengths are identical ($\eta_{ps}^{-1} = \eta^{-1}$), but also that the corresponding coupling parameters are additive: $\ln(M_{ps}) = \ln(A_p) + \ln(A_s)$.

From Eqs. (16) and (19) follows that for extremely dilute supporting electrolytes, namely, when $\mathbf{R}_B \rightarrow \mathbf{0}$, the screening function takes the limiting constant value $\kappa_B^2(k) \approx \kappa_D^2$ ($\equiv 4\pi \ell_b \mathbf{Z}_B^T \mathbf{R}_B \mathbf{Z}_B$), where κ_D^{-1} is the Debye screening length of this supporting electrolyte. Consequently, in this regime occurs that $\eta \approx \kappa_D$ and $E^{(R)} \approx 1$. Indeed, in the standard DLVO theory the Debye-Hückel model is assumed for the supporting electrolyte (i.e., $f(k) = 1$ and $\mathbf{C}_{BB}^s = \mathbf{0}$), so in this instance we have the exact equalities $E^{(R)} = 1$ and $\eta = \kappa_D$. The other ingredients of this theory are that each macroion of species p is modeled as a hard sphere of diameter σ_p, that the correlations between it and the small ions in the supporting electrolyte are linearized, and that $\mathbf{R}_0 = \mathbf{0}$. The resulting expression for the renormalized charges is then[19,20]

$$A_p^{(DLVO)} = \frac{\exp(\kappa_D \sigma_p/2)}{1 + \kappa_D \sigma_p/2} q_p, \quad (25)$$

where q_p is the bare charge in elementary charge units of a macroion of type p. Still within the realm of the Debye-Hückel model, it has been investigated how the renormalized charge is affected either by nonlinear correlations between the macroions and the small ions,[23,33,36] or by finite macroion concentrations $\mathbf{R}_0 \neq \mathbf{0}$,[26,28] as well as by combination of both effects.[25,43]

IV. MODEL SYSTEM AND COMPUTER SIMULATION METHODOLOGY

For simplicity, let us consider a multicomponent ionic solution, treated at the McMillan-Mayer level of description, in which the ionic species are modeled as soft-core charged spheres with point-charges embedded in their centers and immersed in a uniform structureless dielectric background. Hence, the pair interaction between a particle of species i and a particle of species j separated at a distance r is given by

$$\beta u_{ij}(r) = \beta u_{ij}^{rc}(r) + \frac{\ell_b}{r} q_i q_j, \quad (26)$$

with the repulsive core potential modeled as follows: a hard core $\beta u_{ij}^{rc}(r) = \infty$ for $r \leq \Delta_{ij}$, a shifted-truncated Lennard-Jones potential

$$\beta u_{ij}^{rc}(r) = 4 \left[\left(\frac{\sigma}{r - \Delta_{ij}} \right)^{12} - \left(\frac{\sigma}{r - \Delta_{ij}} \right)^6 \right] + 1 \quad (27)$$

for $\Delta_{ij} < r < \Delta_{ij} + 2^{1/6}\sigma$, and by $\beta u_{ij}^{rc}(r) = 0$ for $r \geq \Delta_{ij} + 2^{1/6}\sigma$. The parameter $\Delta_{ij} = (d_i + d_j)/2 - \sigma$ then acts as the hard-core diameter in this interaction, d_i being the effective diameter of species i, whereas σ regulates its hardness. In this way, $\beta u_{ij}^{rc}((d_i + d_j)/2) = 1$ and the form of the potential guarantees a soft continuous repulsion beyond the inner core, that is, for $r > \Delta_{ij}$. In order to mimic the hard core interaction

characteristic of the primitive model, σ is set here equal to 0.1 nm.

Keeping with the simplest scenario for a colloidal suspension, we focus our study to three ionic components: macroions, denoted as species M; anions, denoted as species a; and cations, denoted as species c. The following set of parameter values is considered fixed throughout this work: $\ell_b = 0.71432$ nm, $q_M = -90$, $q_a = -1$, $q_c = +1$, $d_M = 5.1$ nm, and $d_a = 0.3$ nm. And in order to evaluate the effects of the counterion size, two cation diameters are considered: $d_c = 0.5$ nm and $d_c = 1.0$ nm. Furthermore, the subset of observable species encompasses only the macroions, whereas the subset of background species includes both species of small ions, namely, the monovalent anions and cations. Physically, these parameters are associated to a suspension of highly charged coated gold nanoparticles immersed in an aqueous solution of NaOH and TBAOH.[59–62] In this experimental system, it was observed that highly charged nanoparticles coagulate near a concentration of 0.1 M for the electrolyte with the smallest cation, whereas the colloidal suspension remained stable at concentrations exceeding 1 M for larger cations. The physical mechanism behind this enhanced colloidal stability is discussed elsewhere.[63]

Here, our main subject is to study the effective force between two macroions defined by

$$\beta F(r) = -\frac{d}{dr} \beta u_{MM}^{eff}(r), \quad (28)$$

which can be evaluated from computer simulations using the general approach described in a previous work.[54] In summary, a cubic simulation cell with periodic boundary conditions is used to perform molecular dynamics (MD) simulations. Two identical nanoparticles were located at fixed positions along one diagonal of the cubic simulation box, symmetrically with respect to the center of the cell, while surrounded by the freely moving monovalent ions (cations and anions) in such a way that the electroneutrality condition,

$$N_M q_M + N_a q_a + N_c q_c = 0, \quad (29)$$

with $N_M = 2$ is indeed fulfilled in all cases. N_a and N_c are, respectively, the number of anions and cations within the cell (see Figure 1(a)). MD simulations were carried out using the LAMMPS package[64,65] in the NVT ensemble via a Nosé-Hoover thermostat[66,67] at a reduced temperature $T' = k_B T/\varepsilon = 1$, where $\varepsilon = k_B T$ is the thermal energy. The time step used was 0.02τ, where τ is the reduced Lennard-Jones unit of time. The total number of ions $N = N_a + N_c$ used in simulations was around 3200 particles. 10×10^6 MD time steps were used to thermalize the system. The total repulsive core and electrostatic forces acting over each nanoparticle were sampled each 10 MD time steps (in a compromise between efficiency and reduction of time correlations), and between 26 and 52×10^6 of MD time steps were performed to calculate the time average of the forces.

At a given instant, the net force exerted over one nanoparticle, labeled as A and located at the position $\vec{r}_A$, is the sum of the direct force exerted by the other nanoparticle, labeled as B and located at $\vec{r}_B$, plus the sum of the forces exerted by each one of the mobile ions, located, respectively, at the positions
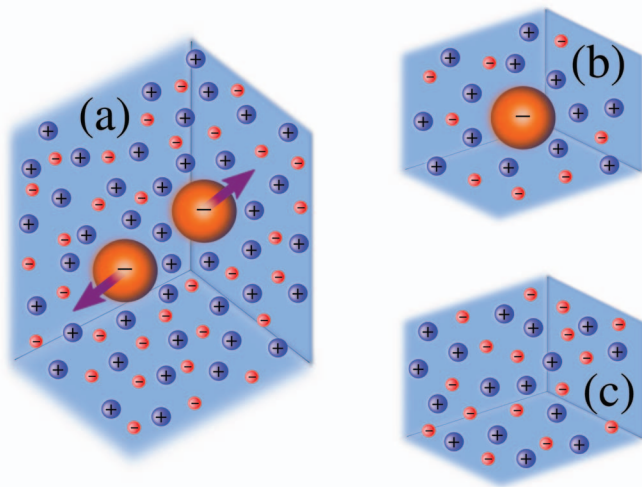
FIG. 1. Monte Carlo simulation setups. (a) Two nanoparticles immersed in a size-asymmetric monovalent electrolyte. (b) A single nanoparticle immersed in a size-asymmetric monovalent electrolyte. (c) The bulk size-asymmetric electrolyte.

$\vec{r}_i^{(\gamma)}$, where $\gamma = a, c$ and $i = 1, 2, \ldots, N_\gamma$. That is, the net force over the macroion A is given by

$$\vec{F}^A(\vec{r}_A) = -\vec{\nabla}_A u_{MM}(|\vec{r}_A - \vec{r}_B|)$$
$$- \sum_{\gamma=a,c} \sum_{i=1}^{N_\gamma} \vec{\nabla}_A u_{M\gamma}(|\vec{r}_A - \vec{r}_i^{(\gamma)}|), \quad (30)$$

where $\vec{\nabla}_A$ denotes the gradient with respect to $\vec{r}_A$. Due to the symmetry of the system, the ensemble average of the net force over the nanoparticle A must lie in the direction of $\vec{r}_A - \vec{r}_B$, and moreover, be a function only of the separation distance between the centers of the two nanoparticles $r = |\vec{r}_A - \vec{r}_B|$. Thus, after averaging over all the configurations, one obtains the corresponding magnitude for the mean force

$$F(r)\hat{r}_{AB} = \langle \vec{F}^A(\vec{r}_A) \rangle, \quad (31)$$

where $\langle \cdots \rangle$ denotes time average in the MD simulations, and $\hat{r}_{AB}$ is the unit vector pointing in the direction from B to A. With these definitions, positive values of $F(r)$ correspond to repulsive mean forces between the nanoparticles, while negative values correspond to attractive mean forces. In order to reduce the effect of random fluctuations at large separation distances, the projection of the resulting time-averaged force over the line joining both nanoparticles was averaged from four independent simulations in all cases. This means that eight different time-averaged forces were used to calculate the final value of $F(r)$ and the corresponding standard deviation, which is a measure of the associated error.

To determine the parameters characterizing the asymptotic behavior of $\beta F(r)$, two other sets of simulations were performed with the same cubic cell, periodic boundary conditions, time step, etc., considered above. In one set, a single nanoparticle was located at the center of the cell in the presence of size-asymmetric monovalent salt (see Figure 1(b)), so $N_M = 1$ in Eq. (29). From this system, the macroion-anion and macroion-cation correlations, $h_{Ma}(r)$ and $h_{Mc}(r)$, respectively, were obtained. The bulk correlations among the small

ions, $h_{aa}(r)$, $h_{ac}(r)$, and $h_{cc}(r)$, were gained from another set of simulations in which no nanoparticle was included (see Figure 1(c)), that is, when $N_M = 0$ in Eq. (29). For consistency, the bulk number densities employed in this last set were matched to the corresponding bulk densities found in the simulations with a single nanoparticle at the center of the cell, namely, the local density values found at the boundaries of the cell, far away from the central macroion (the determination of the corresponding bulk densities for the simulations with two macroions is more difficult since, as discussed ahead, it may depend on the separation distance between macroions). In all these instances, the total number of ions $N = N_a + N_c$ used were around 2000, and between 10 and 20×10^6 of MD time steps were executed to evaluate the correlation functions. For all the simulation configurations illustrated in Figure 1, electrostatic interactions were handled properly via the well established Ewald summation method.

The short-range direct correlation functions $\tilde{c}_{ij}^s(k)$, needed for the determination of η, $E^{(R)}$ and A_M, are then garnered from these simulation data following the ideas proposed by Ulander and Kjellander.[58] Here, we proceed as follows. The multicomponent OZ equations are complemented with the set of closures given by

$$h_{ij}(r) = h_{ij}^{\text{sim}}(r) \quad (32)$$

for $r \leq R_{ij}^c$, where $h_{ij}^{\text{sim}}(r)$ is the total correlation function obtained from the computer simulations, and by

$$h_{ij}(r) = \exp\left(\xi_{ij}^s(r) + b_{ij}^{\text{ext}}(r) - \beta u_{ij}^s(r)\right) - 1 \quad (33)$$

for $r > R_{ij}^c$, where $\xi_{ij}^s(r) = h_{ij}(r) - c_{ij}^s(r)$ is the short-range indirect correlation function and $b_{ij}^{\text{ext}}(r)$ is an extrapolation of the corresponding bridge function obtained in the region $r \leq R_{ij}^c$; Eq. (33) follows directly from Eqs. (3) and (13). If the cutoff distances R_{ij}^c are large enough, the corresponding bridge functions become negligible and different extrapolation approaches yield basically the same results. However, R_{ij}^c cannot be too large since for the canonical ensemble $h_{ij}(r) \sim -N^{-1}$ instead of the grand canonical ensemble asymptotic behavior, $h_{ij}(r) \sim 0$, which underpins the validity of the OZ equations. In practice, the optimal R_{ij}^c are determined by simply requiring that the calculated total correlation functions match the simulated ones in the region just outside the cutoff distance, that is, $h_{ij}(r) \approx h_{ij}^{\text{sim}}(r)$ for $r \gtrsim R_{ij}^c$. To facilitate the numerical calculations, by assuring a fast enough decay of $\tilde{v}(k)$ for large values of k, we assume that $f(k) = \alpha^2/(k^2 + \alpha^2)$ in Eq. (12), so $v(r)$ does not diverge at $r = 0$ and

$$\beta u_{ij}^s(r) = \beta u_{ij}^{rc}(r) + \frac{\ell_b}{r} \exp(-\alpha r) q_i q_j \quad (34)$$

is then the short-range potential used here (with $\alpha^{-1} = 0.02$ nm to make this immaterial parameter smaller than any physical length scale in the model). Further details of the numerical method implemented to solve the multicomponent OZ equations with the closures defined by Eqs. (32) and (33) are provided in Appendix B. Since this approach depends mostly on numerical integrations of the distribution functions obtained from computer simulations, the error bars for the computed values of the screened Coulomb parameters are rather small, usually less than 5%.

The present study is focused on the case of infinite macroion dilution, namely, $\rho_M = 0$ M, and consequently the full set of OZ equations decouple into three subsets. The first subset involves only the bulk correlations among the small ions, and allows us to determine the functions $\tilde{c}^s_{aa}(k)$, $\tilde{c}^s_{ac}(k)$, and $\tilde{c}^s_{cc}(k)$, which in turn, according to Eqs. (16), (19), and (20), fix the values of η and $E^{(R)}$. The second subset includes the correlations between a macroion and the small ions, and is thus applied to the determination of the functions $\tilde{c}^s_{Ma}(k)$ and $\tilde{c}^s_{Mc}(k)$, from where the renormalized charge A_M is then obtained using Eq. (17). The third set relates the macroion-macroion correlation to all the other correlations and can be used to evaluate the bridge functions $b_{MM}(r)$. It should also be pointed out that even though the aim is to emulate the infinite dilution limit, the simulations with one nanoparticle per cell correspond indeed to finite colloidal volume fractions, ranging from 6.69×10^{-5} when $\rho_a \approx 0.002$ M, up to 8.36×10^{-3} for $\rho_a \approx 0.2$ M. Nonetheless, in all cases the box size is much larger than the corresponding screening length, so the effect from the finite volume fraction on the corresponding $g_{Mi}(r)$ for $i = a, c$ is imperceptible, and can be safely neglected.

V. RESULTS

A. Mean forces

The data for $\beta F(r) r^2 / \ell_b$ obtained from the computer simulations described above are represented by the symbols in Figure 2. Three salt concentrations are illustrated: 0.002 M (squares), 0.02 M (circles), and 0.2 M (triangles); whereas panels (a) and (b) correspond, respectively, to $d_c = 0.5$ nm and $d_c = 1.0$ nm. The macroion-macroion effective force clearly displays a crossover from a rapidly decaying short-range regime to the long-range behavior described by the functional form

$$\beta F^{\text{asy}}(r) = \frac{\ell_b A_M^2}{E^{(R)}} \frac{\exp(-\eta r)}{r^2} (1 + \eta r), \qquad (35)$$

which is derived from the Yukawa component of the corresponding EPP, namely, from the second term in the right hand side of Eq. (24). This crossover reflects the characteristic features of the ionic distribution structure around each macroion:[56,57] a counterion rich (coion depleted) region at short distances, roughly corresponding to the Stern layer, but of finite thickness, followed by the diffuse (Gouy-Chapman) region describable by a mean-field theory. Therefore, the bump in $\beta F(r)$ at short separation distances comes from the overlapping of the Stern-like layers surrounding each macroion and the fact that, as the macroions become closer, these layers cannot effectively shield the bare macroion charges.

The onset of the Yukawa force regime, on the other hand, indicates that such overlapping is no longer taking place and, consequently, the interaction is ruled by a screened Coulomb potential with renormalized charges induced by the short-range shielding from the small ions. It is also clear that the counterion size affects not only the thickness of the Stern-like shell, but also the magnitude of the renormalized charge. In fact, as shown below, this size influences the screening
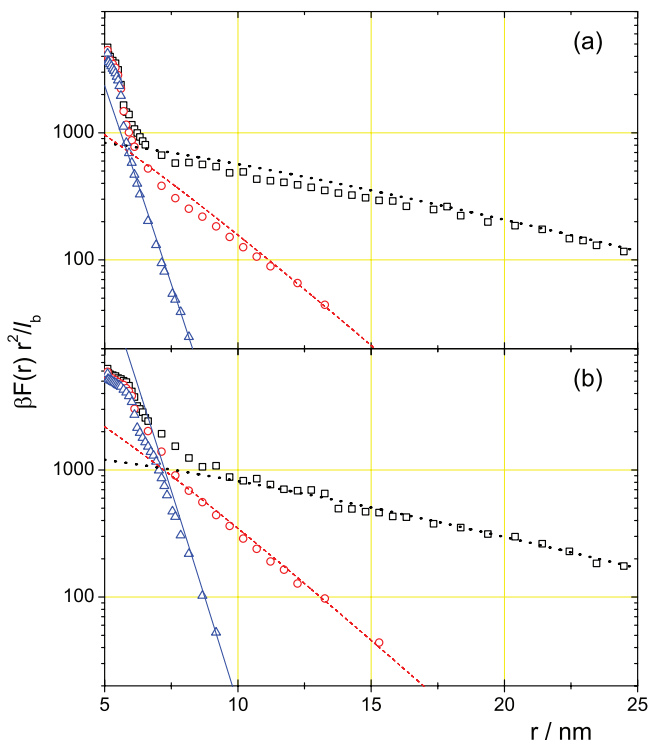
FIG. 2. Mean forces between two identical charged nanoparticles (times the square separation distance) immersed in a 1:1 size-asymmetric electrolyte. The nanoparticles have size $d_M = 5.1$ nm and charge $q_M = -90$, while the anion size is $d_a = 0.3$ nm in all instances. In panel (a), the cation size is $d_c = 0.5$ nm, whereas in panel (b) the cation size is $d_c = 1.0$ nm. In both panels, the following salt concentrations were considered: 0.002 M (squares), 0.02 M (circles), and 0.2 M (triangles). The symbols correspond to MD simulations results (errors are at most of the size of the corresponding symbol), while the lines correspond to Yukawa forces with the parameters given in Table I, whose determination is the main subject of this work.

length and effective permittivity too. Naturally, it is possible to fit the parameters η and $\ell_b A_M^2 / E^{(R)}$ directly from the long-range data for $\beta F(r)$ or $\beta u_{MM}^{\text{eff}}(r)$.[23,33,41,50,52,53,55] Nonetheless, greater insight into the nature of the screened Coulomb parameters, via their connection to the correlations among the small ions and between them and the macroions, can be gained from applying instead the results contained in Eqs. (16)–(22). The lines in Figure 2 represent the results of this endeavor, with the details described next.

B. Screened Coulomb parameters

Table I contains the resulting values for the parameters of the screened Coulomb potential, as well as the corresponding values for the Debye length κ_D^{-1} and the effective charge defined by the standard prescription[23,33,52]

$$A_M = \frac{\exp(\eta S_M)}{1 + \eta S_M} q_M^{eff}, \qquad (36)$$

modeled in Eq. (25), but with η instead of κ_D and $S_M \equiv (d_M + d_c)/2$ instead of $\sigma_M/2$. These last two modifications thus take into account the real screening length and the real distance of closest macroion-counterion approach coming from the finite counterion size, keeping in mind that $E^{(R)} \approx 1$ for all the cases considered. Also reported in this table are the

TABLE I. Parameter values corresponding to the screened Coulomb potential between two macroions immersed in a monovalent electrolyte for the same conditions of Figure 2.

		Asymptotic parameters				
d_c (nm)	ρ_c (M)	κ_D^{-1} (nm)	η^{-1} (nm)	$E^{(R)}$	A_M	q_M^{eff}
0.5	0.002017	6.772	6.774	1.0000	-31.65	-29.59
0.5	0.020250	2.137	2.132	1.0002	-54.76	-34.07
0.5	0.205700	0.6706	0.6315	0.9968	-848.9	-54.73
1.0	0.002020	6.767	6.761	1.0000	-38.01	-35.13
1.0	0.020330	2.133	2.106	1.0001	-83.42	-47.99
1.0	0.209400	0.6646	0.6055	0.9993	-3507	-137.4

number densities used in the corresponding bulk simulations. The first thing to notice is that $\eta^{-1} \approx \kappa_D^{-1}$ for 0.002 M, whereas $\eta^{-1} < \kappa_D^{-1}$ for 0.02 M and 0.2 M, indicating that for sufficiently high salt concentrations the finite ionic size enhances the long-range screening of the electrostatic interactions without perceptibly modifying the effective permittivity of the supporting electrolyte. The differences induced by the cationic size seem to be rather minor in regard to the screening length, the most salient departure occurring for 0.2 M, where $\eta/\kappa_D = 1.062$ for $d_c = 0.5$ nm, while $\eta/\kappa_D = 1.098$ for $d_c = 1.0$ nm.

The influence of the counterion size is clearly more conspicuous with regard to the renormalized charge, where the values of $|q_M^{eff}|$ are larger for the cases with $d_c = 1.0$ nm than for the cases with $d_c = 0.5$ nm at comparable salt concentrations. The form and parameter choices of Eq. (36) are designed to minimize the impact of the counterion size, so this fact is rather remarkable and highlights the importance of the unequal charge neutralization mechanism.[68] Furthermore, whereas $|q_M^{eff}| < |q_M|$ in most cases, in accord with the usual expectation that nonlinear effects shield the bare macroion charge,[23,33,55] for the largest counterion at the highest concentration we have instead that $|q_M^{eff}| > |q_M|$, indicating that at high enough ionic strengths such mechanism is even capable of inducing charge amplification. In this last case, the swelling of the Stern-like layer induced by the larger counterions seems to allow a relatively larger adsorption of coions on the macroion surface, thus prompting a reduced shielding of the bare charge. Let us also point out that if κ_D and $d_M/2$ are used in Eq. (36) instead of η and S_M, respectively, this amplification becomes more dramatic, affecting at high salt concentrations even the case with the smallest counterions, so it does not seem to be an artifact of the adjusting scheme. This is shored up by the analysis presented in Subsection V C.

The lines in Figure 2 represent the plots of Eq. (35) with the parameter values given in Table I (dotted lines for $\rho_a \approx 0.002$ M, dashed lines for $\rho_a \approx 0.02$ M, and solid lines for $\rho_a \approx 0.2$ M). Clearly, these lines fit the corresponding mean forces for large enough separation distances, and deviate markedly from these forces only for $r \lesssim d_M + 2d_c$. The smaller discrepancies observed at larger distances, especially for the smallest counterions at low salt concentrations, are explained, in part, by the dependence of the corresponding bulk densities on the separation between macroions (MD simulations were not performed at constant chemical potential).

Close to contact, where the bare macroion charge is only partially shielded by the Stern-like layers and the depletion forces become more important, the mean forces corresponding to the same counterion size but different ionic strengths assume similar shapes with nearly identical contact values $\beta F(d_M)$. The size of the counterions, on the other hand, affect not only this contact value but, most noticeable, the breadth of the short-range bulge on the graphs of the mean forces.

C. Renormalized charge distributions

Our understanding of the mechanisms regulating the renormalization of macroion charges, and, in particular, the source of the charge magnification phenomena, can be deepened by looking at the nature of the renormalized charge distribution associated with each macroion. From Eqs. (16) and (17) it follows that

$$z_M^{(R)}(r) = q_M \delta(\vec{r}) + \Delta z_M^{(R)}(r), \qquad (37)$$

where

$$\Delta z_M^{(R)}(r) = g_{Ma}^{(R)}(r) \rho_a q_a + g_{Mc}^{(R)}(r) \rho_c q_c, \qquad (38)$$

with the functions $g_{Mi}^{(R)}(r)$ given by the density expansion

$$\tilde{g}_{Mi}^{(R)}(k) = \tilde{c}_{Mi}^s(k) + \sum_{p=a,c} \tilde{c}_{Mp}^s(k) \rho_p \tilde{c}_{pi}^s(k)$$
$$+ \sum_{p=a,c} \sum_{q=a,c} \tilde{c}_{Mp}^s(k) \rho_p \tilde{c}_{pq}^s(k) \rho_q \tilde{c}_{qi}^s(k) + \cdots$$
$$(39)$$

in Fourier space. These functions can be interpreted as virtual (short-ranged) distribution functions that can take not only positive but also negative values. The first term on the right hand side of Eq. (39) corresponds to the short-range direct correlation between the macroion and the small ions, while successive terms represent indirect short-range macroion-ion correlations mediated by ever more extended short-range ion-ion correlations. The renormalized macroion charge is then given by

$$A_M = q_M + 4\pi \int_0^\infty dr\, r^2\, i_0(\eta r)\, \Delta z_M^{(R)}(r), \qquad (40)$$

where $i_0(x) \equiv \sinh(x)/x$ is the spherical modified Bessel function of order zero. This last relationship is meaningful as long as $i_0(\eta r) \Delta z_M^{(R)}(r)$ decays fast enough with increasing r, which is always the case for the situations under consideration in this work.

Figures 3 and 4 illustrate the behavior of $4\pi \ell_b r^2 \Delta z_M^{(R)}(r)$ (solid line), and its corresponding anionic ($4\pi \ell_b r^2 g_{Ma}^{(R)}(r) \rho_a q_a$, dotted line) and cationic ($4\pi \ell_b r^2 g_{Mc}^{(R)}(r) \rho_c q_c$, dashed line) components, for the cases $\rho_a \approx 0.02$ M and $\rho_a \approx 0.2$ M, respectively. In both figures, panel (a) corresponds to $d_c = 0.5$ nm whereas panel (b) corresponds to $d_c = 1.0$ nm. The factor ℓ_b was introduced to make these quantities dimensionless, though since $\ell_b \approx 1$ nm in our system, the data presented are basically the local charges in elementary units. The first thing to notice is that $\Delta z_M^{(R)}(r) \neq 0$ for $r < (d_M + d_a)/2$ in all cases. Furthermore,
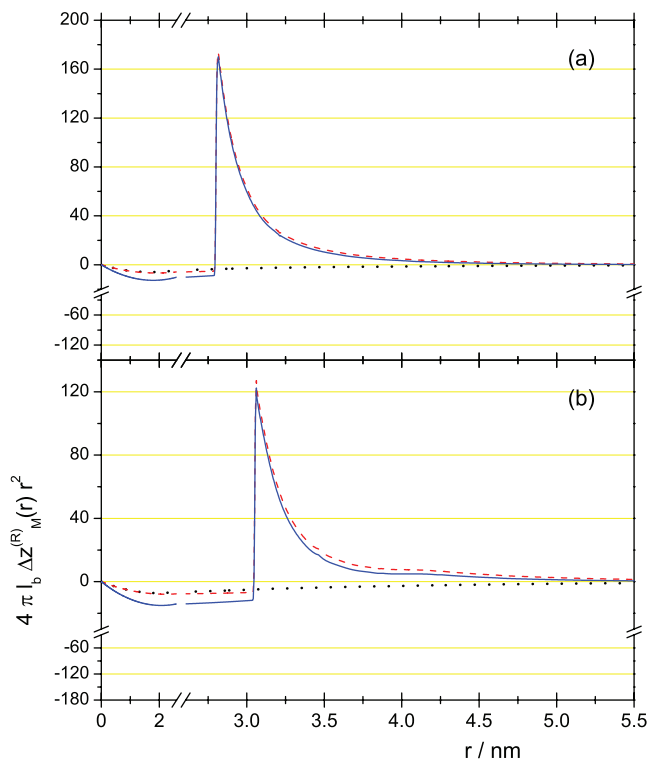
FIG. 3. Renormalized charged distributions times $4\pi \ell_b r^2$ (solid lines), and the corresponding cationic (dashed line) and anionic (dotted line) components, for 0.02 M. Panel (a) is for $d_c = 0.5$ nm, panel (b) is for $d_c = 1.0$ nm.
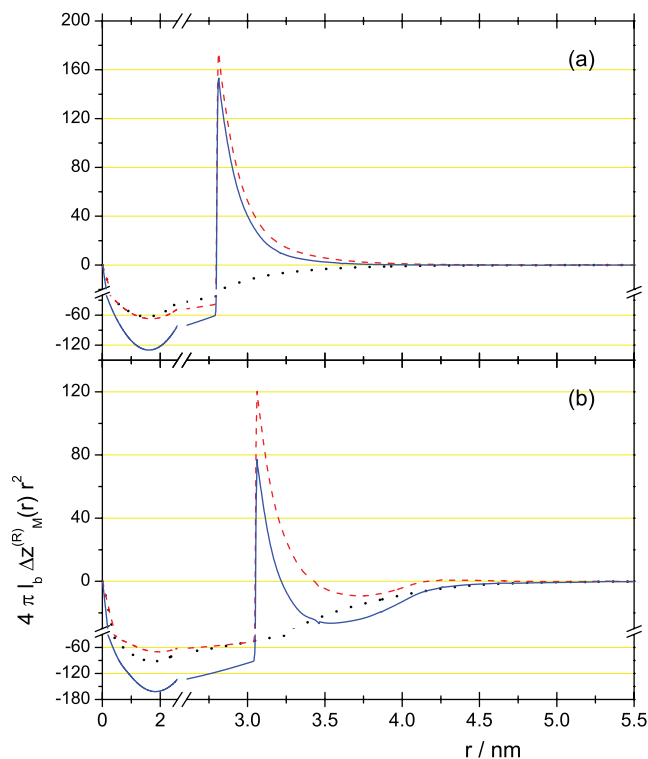
FIG. 4. Renormalized charged distributions times $4\pi \ell_b r^2$ (solid lines), and the corresponding cationic (dashed line) and anionic (dotted line) components, for 0.2 M. Panel (a) is for $d_c = 0.5$ nm, panel (b) is for $d_c = 1.0$ nm.

$g_{Ma}^{(R)}(r) > 0$ for the same range, while $g_{Mc}^{(R)}(r) < 0$ for $r < (d_M + d_c)/2$. This negative short-range distribution of counterions inside the macroion, together with the positive short-range distribution of coions in the same region, reinforces the bare macroion charge and explains why $|A_M| > |q_M|$. Indeed, the same situation applies to the approximations involved in the DLVO model. The first factor on the right hand side of Eq. (25) is originated precisely by the fact that, even though $\Delta z_M^{(R)}(r) = 0$ for $r > \sigma_p/2$ in this approximated scheme, $\Delta z_M^{(R)}(r)$ inside the macroion is nonzero, and actually shows the same attributes discussed above: negative (positive) virtual distributions for counterions (coions) inside the colloid.[57] Moreover, this is the case for any approach in which the correlations between the macroion and the point ions are linearized.[26, 32, 52] The real distributions $g_{Mi}(r)$ are, of course, null inside the macroion, but the virtual distributions $g_{Mi}^{(R)}(r)$ emerge from the difference between those real distributions and the long-range components that determine their asymptotic behavior.[56, 57] The negative values of the virtual counterion distributions thus seem to emerge, in a rather simplistic explanation, from the necessity to compensate for the absence of counterions inside the macroion; counterions that a linearized mean-field approach would otherwise require to be present in that region. For the system discussed here, it seems safe to assume that these features are mostly taken into account by the first factor on the right hand side of Eq. (36). As the supporting electrolyte concentration increases, the magnitude of $\Delta z_M^{(R)}(r)$ for $r < (d_M + d_c)/2$ also grows up, and consequently this factor becomes bigger.

Complementarily, the influence of the renormalized charge distribution in the region outside the repulsive core of the macroion, corresponding to the Stern-like layer with finite width mentioned above, is mostly accounted for by the effective charge q_M^{eff}. In this regard, the contact value of the virtual counterion distribution, $g_{Mc}^{(R)}((d_M + d_c)/2)$, remains basically invariant as the electrolyte concentration varies (even for 0.002 M, not shown), whereas the virtual distribution of coions exhibits a more noticeable evolution, with $g_{Ma}^{(R)}(r) > 0$ for all separation distances, but decidedly rising in magnitude as the concentrations increases. The magnitude of $\Delta z_M^{(R)}((d_M + d_c)/2)$, which is positive, consequently decreases with increasing electrolyte concentration. The net contribution from $\Delta z_M^{(R)}(r)$ for $r > (d_M + d_c)/2$ is of the opposite sign to the bare charge in most cases, explaining why $|q_M^{eff}| < |q_M|$ in these situations. The exception is, indeed, the case corresponding to 0.2 M and $d_c = 1.0$ nm, where clearly $\Delta z_M^{(R)}(r) < 0$ for $r \gtrsim 3.22$ nm. This yields the augmentation that induces $|q_M^{eff}| > |q_M|$, especially since the factor $i_0(\eta r)$ in the integrand in Eq. (40) gives a greater weight to this region than to the region in the immediate vicinity of the macroion. It is also interesting to look at how much of this augmentation comes from each component. For sufficiently low electrolyte concentrations, the virtual distribution of counterions is always positive outside the macroion, that is, $g_{Mc}^{(R)}(r) > 0$ for $r > (d_M + d_c)/2$, and this is still true for $\rho_a \approx 0.2$ M when $d_c = 0.5$ nm. For $d_c = 1.0$ nm at the same high electrolyte concentration, however, $g_{Mc}^{(R)}(r)$ becomes negative within the region 3.43 nm $< r <$ 4.16 nm, and, moreover, seems to have an

oscillatory behavior beyond this point. But the largest contribution to the macroion charge augmentation comes from the virtual distribution of coions in the immediate vicinity of the macroion, where we have that $4\pi \ell_b \, r^2 \, g_{Ma}^{(R)}(r) \, \rho_a \, q_a \approx -44$ for $r = (d_M + d_c)/2$, thus adding a considerable amount of negative charge to A_M.

D. Bridge functions

The approach used here allows, too, the determination of all the bridge functions in the system by using Eq. (3), at least outside the regions where $g_{ij}(r) = 0$. The bulk bridge functions $b_{aa}(r)$, $b_{ac}(r)$, and $b_{cc}(r)$, not shown here, have a magnitude of less than 0.14 for all the cases considered, with the maximum occurring at contact for the highest dilution, and decay rapidly with increasing separation distances. The well-known hyper-netted chain (HNC) approximation, which neglects the bridge functions for all separation distances, thus provides a fairly good description of the correlations in the bulk electrolyte. For the correlations between macroions and small ions, on the other hand, the HNC approach does not provide a suitable description, and even fails to converge for the most dilute cases. Figure 5 illustrates in inverted scale the corresponding bridge functions $b_{Mc}(r)$ (main) and $b_{Ma}(r)$ (inset) for the cases: $\rho_a \approx 0.002$ M (dotted lines), $\rho_a \approx 0.02$ M (dashed lines), and $\rho_a \approx 0.2$ M (solid lines); where panels (a) and (b) correspond, respectively, to $d_c = 0.5$ nm and $d_c = 1.0$ nm. The noisy regions on the plots of $b_{Ma}(r)$ are due to the fact that $g_{Ma}(r) \approx 0$ in those regions, which is exacerbated by the logarithm in Eq. (3). These are, however,
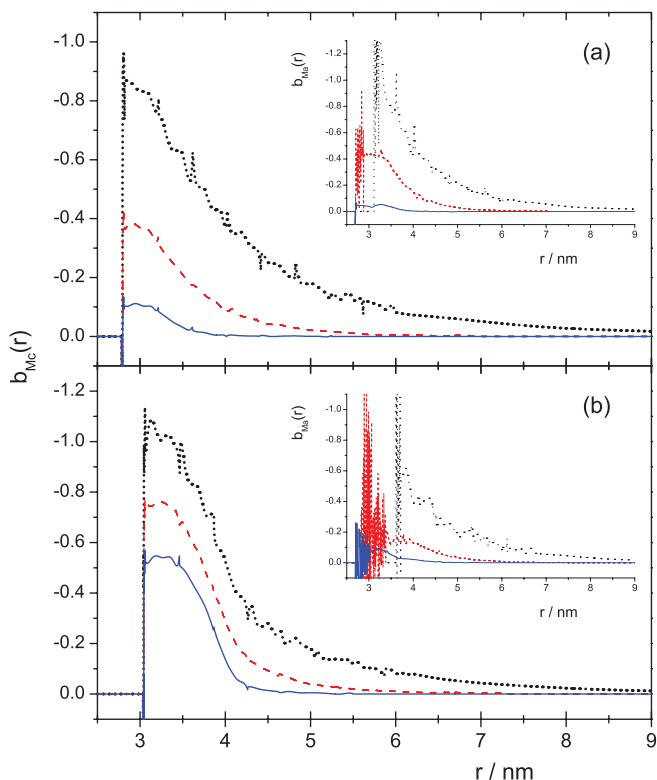
FIG. 6. (a) and (b) Bridge functions for the macroion-macroion correlations for the same conditions as in Figure 2.

precisely the regions where the repulsive potential dominates the behavior of this distribution function, thus making rather irrelevant the contribution from the corresponding bridge function. Regarding the central goal of this work, the main conclusion here is that $b_{Mc}(r)$ and $b_{Ma}(r)$ enhance the corresponding short-range repulsions, when compared to the HNC approximation, thus affecting the ensuing renormalized charges.

Having ascertained the behavior of $F^{\mathrm{asy}}(r)$, it is now possible to integrate numerically the short-range mean force $F^*(r) \equiv F(r) - F^{\mathrm{asy}}(r)$ to obtain the potential of mean force $\beta w_{MM}(r) \equiv -\ln(1 + h_{MM}(r))$ between the macroions. Feeding this information into Eq. (3) allows us to determine the corresponding macroion-macroion bridge function. The results obtained from this exercise are illustrated in Figure 6, where the plots of $-b_{MM}(r)$ are reported. The notation is the same as in the previous figure. The net effect is an enhanced macroion-macroion repulsion at short distances, which becomes more important as the electrolyte concentration decreases. Once more, as has been previously observed,[49] the HNC approach is not reliable under these conditions, even when it converges.

VI. CONCLUDING REMARKS

A direct fit of the EPP long-range behavior[23,33,41,50,52,53,55] runs into various problems. On the one hand, it is difficult to estimate in advance at what separation distance between macroions the non-asymptotic term becomes negligible enough; part of the problem being the lack of prior knowledge about the cutoff distance

FIG. 5. (a) and (b) Bridge functions for the correlations between macroions and small ions for the same conditions as in Figure 2.

at which $\Delta z_M^{(R)}(r)$ becomes sufficiently small.[52] For too large separation distances, on the other hand, the general uncertainty in the data increases. A separate issue occurs in particular for computer simulation studies, which are seldom implemented at constant chemical potentials. This may be especially troublesome for situations, as ours, in which two macroions are kept at fixed positions while the small ions are let to move freely within the cell. The region between the macroions at intermediate separation distances is thus prone to be overpopulated by counterions and depleted of coions, leaving the rest of the cell with counterion excesses and coion deficiencies. Hence, different separation distances may actually correspond to different bulk densities. This lack of consistency with regard to the implicit chemical potentials is also a problem when comparing simulations corresponding to dissimilar macroion species, even when the number of small ions in the cell is kept fixed. The small disagreements in bulk densities seem to have relatively minor effects on the screening lengths, which depend roughly on the inverse square root of these densities, but large consequences on the effective charges, due mostly to the exponential in the first factor on the right hand side of Eq. (36). These difficulties may explain the apparent non-additivity of the renormalized charges reported by Allahyarov and Löwen.[50] By contrast, the dressed ion theory provides exact and robust techniques for determining these asymptotic parameters, which allow us to minimize, or even shunt altogether, many of these problems. This is so because the main input for these techniques are the short-range components of the correlations, which are usually easier to ascertain. Furthermore, the resulting values are obtained by numerical integrations, which are less sensitive to data noise. The additivity of the renormalized charges, for example, which in the limit of infinite macroion dilution at fixed bulk electrolyte densities seems rather straightforward, is guaranteed in the most general case by the fact that these parameters depend only on the short-ranged distributions of the small ions around a single macroion, as portrayed by Eqs. (37)–(40).

The usefulness of the different theoretical approaches available for the determination of the screened Coulomb parameters may be tested against the benchmark provided by the corresponding values attained directly from computer simulation studies using the method proposed in this work. For example, we can compare the results reported here against the renormalized charges $A_M^{(PB)}$ obtained from the well-established PB equation in the case corresponding to a spherical macroion immersed in an infinite sea of point ions at finite salt concentration (thus requiring a vanishing electrostatic potential at $r \to \infty$). Within the framework employed here, this approach is exactly equivalent to assuming that $\rho_M = 0$, $\alpha^{-1} = 0$, $b_{iM}(r) = b_{Mi}(r) = 0$ for $i = a, c$, and $c_{ij}^s(r) = 0$ for $i, j = a, c$; consequently, $\eta = \kappa_D$ and $E^{(R)} = 1$. To make the comparison more meaningful, we consider here the asymmetric hard-core conditions $g_{iM}(r) = g_{Mi}(r) = 0$ when $r < (d_M + d_i)/2$ for $i = a, c$. The renormalized charges obtained for the cases of $\rho_a \approx 0.02$ M with $d_c = 0.5$ nm and $d_c = 1.0$ nm, for example, are $A_M^{(PB)} = -59.82$ and $A_M^{(PB)} = -70.16$, respectively. In this instance, the mean-field approach overestimates the renormalized charge corresponding to the smallest

counterions, but underestimates it in the case with the largest counterions. When $\rho_a \approx 0.2$ M, on the other hand, $A_M^{(PB)} = -712.2$ for $d_c = 0.5$ nm, whereas $A_M^{(PB)} = -1080$ for $d_c = 1.0$ nm; so in this occasion the renormalized charges are underestimated in both cases, patently more so for the largest counterions. Thus, the PB equation provides a computationally less demanding approach that captures the main features of this type of systems by providing a reasonable description of the trends in the behavior of A_M as a function of the counterion size, at least for weakly coupled systems. On the other hand, the PB approach seems to predict an effective charge augmentation for infinite cylindrical macroions immersed in an electrolyte with divalent coions and univalent counterions, at least for certain asymptotic limits,[45] although the underlying mechanism is rather different from the one studied here.

The insights gained from the type of analysis described in this work should allow a richer and deeper understanding of the experimental data gathered from the physicochemical systems under consideration. Optical microscopy and light scattering techniques, for example, provide direct information on the colloidal correlations by measuring the corresponding colloidal distribution function $g(r)$, in the case of the former, or its Fourier transform, the colloidal structure factor $S(k)$, in the case of the latter. Although the data are often presented in terms of the potential of mean force $w(r) \equiv -k_B T \ln g(r)$, it is more sensible to analyze the structural properties in terms of the corresponding EPP, since it explicitly excludes misleading many-body effects;[25–27, 36] in the limit of infinite macroion dilution the effective interaction $u^{\text{eff}}(r)$ becomes indeed equivalent to the potential of mean force $w(r)$. Optical microscopy can also provide a more direct description of the EPP, by tracking the trajectories of two neighboring colloidal particles moving freely,[9, 14] or even by manipulating them directly by means of optical tweezers.[10, 13] Under some of these experimental conditions, the large colloids may not be at thermal equilibrium, but the solvent molecules and small ions in the supporting electrolyte are fast relaxing components that equilibrate rapidly for a given colloidal distribution. The measured EPP should then be comparable to those obtained from theoretical schemes. For computer simulation studies at the McMillan-Mayer level of description, on the other hand, the contribution from such fast relaxing small ions can be easily summed up for each fixed distribution of the colloids in the solution. The slow evolution of the colloidal distribution, however, may render these simulations impractical for the study of long term processes. The theoretical EPPs can then be used too for more economical computer simulations.

The usual claim that the DLVO model has been experimentally confirmed just means, for the most part, that the long range screened Coulomb term in Eq. (24) accurately fits the relevant experimental data for sufficiently dilute colloidal suspensions. Traditionally, the information thus obtained has been interpreted by using the standard DLVO result for the renormalized charge, namely, Eq. (25), thus producing *ad hoc* values of the corresponding screening lengths and macroion bare charges. However, a better fit of these fundamental physical parameters can be attained by using the more sophisticated techniques discussed here. In particular, the DLVO model predicts that, at a given ionic strength, the renormalized charges

are independent of the nature of the small ions. Contrary to this, the theoretical approaches examined here indicate that changing the type of added salt, while keeping the same solvent and colloidal particles, should induce different degrees of renormalization in the effective charges of the macroions, as well as modify their short-range interactions; these effects may help to explain recent experimental results.[59,69] Other important issues that may be considered in future theoretical studies about effective macroion interactions are multivalent small ions and polarization effects.[70–76]

APPENDIX A: EFFECTIVE DIRECT CORRELATION FUNCTIONS

We shall start by considering the grand canonical description of the static properties of a multicomponent fluid. Thus, our system is composed by M different species of particles confined inside a finite region, where N_α and μ_α are, respectively, the number of particles of species α in a given configuration and the corresponding chemical potential. In that same microscopic configuration, $\mathbf{r}_i^{(\alpha)}$ is the position of the ith particle of species α. To simplify the notation, we denote by $\vec{N}$ and $\vec{\mu}$ the M-vectors constituted, respectively, by the numbers of particles and the chemical potentials. The average value of any function $\hat{A}(\{N\}; \{\mathbf{r}\})$ of the particles positions (a classical operator which depends on the microscopic configuration) is then given by

$$\langle \hat{A} \rangle = \Xi^{-1} \, \mathrm{Tr} \, \hat{f} \, \hat{A}, \tag{A1}$$

where

$$\hat{f}(\{N\}; \{\mathbf{r}\}) = \exp[\beta \vec{\mu} \cdot \vec{N} - \beta \, \hat{V}(\{N\}; \{\mathbf{r}\})] \tag{A2}$$

is the unnormalized probability density,

$$\Xi = \mathrm{Tr} \, \hat{f} \tag{A3}$$

is the grand partition function that normalizes this density, and the standard notation

$$\mathrm{Tr} \, \hat{A} = \sum_{\{\vec{N}\}} \left[\prod_{\alpha=1}^{M} N_\alpha! \, \Lambda_\alpha^{3N_\alpha} \right]^{-1} \int d\{\mathbf{r}\} \, \hat{A}(\{N\}; \{\mathbf{r}\}) \tag{A4}$$

denotes the classical trace of the operator $\hat{A}(\{N\})$. The sum is realized over all possible numbers of particles (i.e., each N_α runs from 0 to infinite), Λ_α is the de Broglie thermal wavelength of species α, and $\hat{V}(\{N\}; \{\mathbf{r}\})$ is the potential energy of a given microscopic configuration. This last operator must be invariant when any two particles of the same species interchange positions (i.e., under $\mathbf{r}_i^{(\alpha)} \leftrightarrow \mathbf{r}_j^{(\alpha)}$).

Let us now consider again the distinction between the m observable species, denoted by the sub-index O, and

the $M - m$ background (unobservable) species, denoted by the sub-index B. Accordingly, we have that $\hat{A}(\{N\}; \{\mathbf{r}\}) = \hat{A}(\{N\}_O; \{\mathbf{r}\}_O; \{N\}_B; \{\mathbf{r}\}_B)$, $\vec{\mu} \cdot \vec{N} = \vec{\mu}_O \cdot \vec{N}_O + \vec{\mu}_B \cdot \vec{N}_B$, and

$$\mathrm{Tr} \, \hat{A} = \mathrm{Tr}_O \, \mathrm{Tr}_B \, \hat{A}, \tag{A5}$$

where

$$\mathrm{Tr}_X \, \hat{A} = \sum_{\{\vec{N}_X\}} \left[\prod_{\alpha \in X} N_\alpha! \, \Lambda_\alpha^{3N_\alpha} \right]^{-1} \int d\{\mathbf{r}\}_X \, \hat{A}(\{N\}; \{\mathbf{r}\}) \tag{A6}$$

for $X = O, B$. Of particular interest in this context are the operators that depend only on the variables of the observable species: $A_O(\{N\}_O; \{\mathbf{r}\}_O)$. The ensemble average of such an operator can then be expressed as

$$\langle \hat{A}_O \rangle = \Xi^{-1} \, \mathrm{Tr}_O \, \hat{f}_O \, \hat{A}_O, \tag{A7}$$

where the unnormalized probability density of the observable subsystem is defined by

$$\hat{f}_O = \mathrm{Tr}_B \, \hat{f}, \tag{A8}$$

and, most importantly, the normalization factor is still given by the same grand partition function defined in Eq. (A3), since $\mathrm{Tr}_O \, \hat{f}_O = \mathrm{Tr}_O \, \mathrm{Tr}_B \, \hat{f} = \mathrm{Tr} \, \hat{f}$. Taking into account that the connection with thermodynamics is given through $\exp(-\beta \Omega) = \Xi$, where Ω is the Landau potential of the original (whole) system, this implies that $\Omega_O = \Omega$, where Ω_O ($\equiv \beta^{-1} \ln[\mathrm{Tr}_O \, \hat{f}_O]$) is the Landau potential of the observable subsystem. To this subsystem corresponds then the effective potential energy $\hat{V}_O^{\mathrm{eff}}(\{N\}_O; \{\mathbf{r}\}_O)$, defined by

$$\hat{f}_O(\{N\}_O; \{\mathbf{r}\}_O) = \exp\left[\beta \vec{\mu}_O \cdot \vec{N}_O - \beta \, \hat{V}_O^{\mathrm{eff}}(\{N\}_O; \{\mathbf{r}\}_O)\right], \tag{A9}$$

and from now on it could be considered as a complete system by itself. In other words, the effective potential energy obtained after integrating out the degrees of freedom of the unobservable species provides us with a contracted description of the system that involves only the observable species. The implications from this viewpoint of a contracted system, with emphasis on two-point correlations, are discussed next.

In order to define these correlations, we start by assuming, as customary, that the potential energy of the whole system is of the form

$$\hat{V}(\{N\}; \{\mathbf{r}\}) = \hat{U}(\{N\}; \{\mathbf{r}\}) + \sum_{\alpha=1}^{M} \int d\mathbf{x} \, \hat{\rho}_\alpha(\mathbf{x}) \, \psi_\alpha(\mathbf{x}), \tag{A10}$$

where we have introduced the local density operator for species α

$$\hat{\rho}_\alpha(\mathbf{x}) = \sum_{i=1}^{N_\alpha} \delta(\mathbf{x} - \mathbf{r}_i^{(\alpha)}). \tag{A11}$$

Hence, for a given intrinsic potential energy $\hat{U}(\{N\}; \{\mathbf{r}\})$, all the thermodynamic quantities can be seen as functionals of the set of external functions $y_\alpha(\mathbf{x})$ defined by

$$y_\alpha(\mathbf{x}) \equiv \mu_\alpha - \psi_\alpha(\mathbf{x}) \tag{A12}$$

(which play the role of local chemical potentials), and immediately follows that

$$\frac{\delta \Omega}{\delta y_\alpha(\mathbf{x})} = -\rho_\alpha(\mathbf{x}) \tag{A13}$$

for $\alpha = 1, \ldots, M$, where $\rho_\alpha(\mathbf{x}) = \langle \hat{\rho}_\alpha(\mathbf{x}) \rangle$ is the equilibrium local number density of particles of species α located in the vicinity of $\mathbf{x}$. Furthermore,

$$\frac{1}{\beta} \frac{\delta \rho_\alpha(\mathbf{x}_1)}{\delta y_\gamma(\mathbf{x}_2)} = -\frac{1}{\beta} \frac{\delta^2 \Omega}{\delta y_\alpha(\mathbf{x}_1)\,\delta y_\gamma(\mathbf{x}_2)}$$
$$= \rho_\alpha(\mathbf{x}_1)\,\rho_\gamma(\mathbf{x}_2)\,h_{\alpha\gamma}(\mathbf{x}_2, \mathbf{x}_2)$$
$$+ \rho_\alpha(\mathbf{x}_1)\,\delta_{\alpha\gamma}\,\delta(\mathbf{x}_1 - \mathbf{x}_2) \tag{A14}$$

for $\alpha, \gamma = 1, \ldots, M$, where $h_{\alpha\gamma}(\mathbf{x}_1, \mathbf{x}_2)$ is the total correlation function between particles of species α and γ located at points $\mathbf{x}_1$ and $\mathbf{x}_2$, respectively. Replacing Ω (viewed as a functional of $\{y\}$) by Ω_O (viewed as a functional of $\{y\}_O$ and $\{y\}_B$ in these last two equations gives us the corresponding relations for the contracted description, but now with $\alpha, \gamma = 1, \ldots, m$. Since $\Omega_O = \Omega$, the equilibrium densities and total two-point correlation functions of this contracted system are identical to those of the original system (not really surprising, given that $\hat{V}_O^{\mathrm{eff}}$ was designed to do precisely this).

Our main interest now is the (inhomogeneous) OZ equation corresponding to the contracted system, which can be obtained by following the same approach used to obtain the OZ equation corresponding to the whole system. Taking into account Eq. (A13) (but with Ω_O instead of Ω), we define the intrinsic free energy $\mathcal{F}_O$ of the contracted system by the (incomplete) Legendre transformation

$$\mathcal{F}_O = \Omega_O + \sum_{\alpha=1}^m \int d\mathbf{x}\,\rho_\alpha(\mathbf{x})\,y_\alpha(\mathbf{x}), \tag{A15}$$

from which follows that $\mathcal{F}_O$ is a functional of $\{\rho\}_O$ and $\{y\}_B$ such that

$$\frac{\delta \mathcal{F}_O}{\delta \rho_\alpha(\mathbf{x})} = y_\alpha(\mathbf{x}) \tag{A16}$$

for $\alpha = 1, \ldots, m$. Next, the excess part of $\mathcal{F}_O$ is obtained through the relation

$$\beta \mathcal{F}_O^{\mathrm{ex}} = \beta \mathcal{F}_O - \sum_{\alpha=1}^m \int d\mathbf{x}\,\rho_\alpha(\mathbf{x}) \left[\ln\left(\Lambda_\alpha^3\,\rho_\alpha(\mathbf{x})\right) - 1 \right], \tag{A17}$$

so the effective direct correlation function of the contracted system is immediately given by

$$c_{\alpha\gamma}^{\mathrm{eff}}(\mathbf{x}_1, \mathbf{x}_2) = -\beta \frac{\delta^2 \mathcal{F}_O^{\mathrm{ex}}}{\delta \rho_\alpha(\mathbf{x}_1)\,\delta \rho_\gamma(\mathbf{x}_2)}. \tag{A18}$$

From Eqs. (A16) and (A17) it then follows that

$$\beta \frac{\delta y_\alpha(\mathbf{x}_1)}{\delta \rho_\gamma(\mathbf{x}_2)} = \frac{1}{\rho_\alpha(\mathbf{x}_1)}\,\delta_{\alpha\gamma}\,\delta(\mathbf{x}_1 - \mathbf{x}_2) - c_{\alpha\gamma}^{\mathrm{eff}}(\mathbf{x}_1, \mathbf{x}_2) \tag{A19}$$

for $\alpha, \gamma = 1, \ldots, m$. Inserting Eqs. (A14) and (A19) into the relationship

$$\sum_{\zeta=1}^m \int d\mathbf{x}_3 \frac{\delta y_\alpha(\mathbf{x}_1)}{\delta \rho_\zeta(\mathbf{x}_3)} \frac{\delta \rho_\zeta(\mathbf{x}_3)}{\delta y_\gamma(\mathbf{x}_2)} = \delta_{\alpha\gamma}\,\delta(\mathbf{x}_1 - \mathbf{x}_2) \tag{A20}$$

yields the desired result

$$h_{\alpha\gamma}(\mathbf{x}_1, \mathbf{x}_2)$$
$$= c_{\alpha\gamma}^{\mathrm{eff}}(\mathbf{x}_1, \mathbf{x}_2) + \sum_{\zeta=1}^m \int d\mathbf{x}_3\, c_{\alpha\zeta}^{\mathrm{eff}}(\mathbf{x}_1, \mathbf{x}_3)$$
$$\times \rho_\zeta(\mathbf{x}_3)\,h_{\zeta\gamma}(\mathbf{x}_3, \mathbf{x}_2) \tag{A21}$$

for $\alpha, \gamma = 1, \ldots, m$.

The procedure to obtain the OZ equation for the whole system is identical to the one just described, but using Ω, $\mathcal{F}$, and $\mathcal{F}^{\mathrm{ex}}$ instead of Ω_O, $\mathcal{F}_O$, and $\mathcal{F}_O^{\mathrm{ex}}$. The definitions of $\mathcal{F}$ and $\mathcal{F}^{\mathrm{ex}}$ parallel those provided in Eqs. (A15) and (A17), but the sums run now all the way up to $\alpha = M$. This means that the interpretation of Eq. (A16), pertaining to the contracted system, and its analogous for the whole system, with $\mathcal{F}$ instead of $\mathcal{F}_O$, are somehow different. In the contracted system, $y_\alpha(\mathbf{x})$ is a functional of $\{\rho\}_O$ and $\{y\}_B$; for the whole system, on the other hand, it is a functional of $\{\rho\}$, namely, the full set of equilibrium densities. This means that in Eq. (A19) the equilibrium density $\rho_\gamma(\mathbf{x})$ is varied while the $\rho_\eta(\mathbf{x})$ for $1 \leq \eta \neq \gamma \leq m$ and the $y_\zeta(\mathbf{x})$ for $m + 1 \leq \zeta \leq M$ are kept fixed, whereas in the equivalent relation for the whole system (where $c_{\alpha\gamma}^{\mathrm{eff}}(\mathbf{x}_1, \mathbf{x}_2)$ is replaced by $c_{\alpha\gamma}(\mathbf{x}_1, \mathbf{x}_2)$) the corresponding variation in $\rho_\gamma(\mathbf{x})$ is carried away while keeping all the remaining $\rho_\eta(\mathbf{x})$ fixed. This explains why in Eq. (A21) the sum in ζ runs just from 1 to m, whereas for the analogous relationship pertaining to the full description of the whole system, the sum in ζ runs all the way up to $\zeta = M$, with α, $\gamma = 1, \ldots, M$.

Finally, the thermodynamic limit, in which the canonical and grand canonical ensembles become equivalent, amounts to taking, for all α, the limit $\psi_\alpha(\mathbf{x}) \to 0$ everywhere (the region of confinement becomes then of infinite extension), while keeping all the chemical potentials fixed. Consequently, $N_\alpha \to \infty$ in such a way that $\rho_\alpha(\mathbf{x}) = \rho_\alpha$, whereas the two-point correlations take the form $h_{\alpha\gamma}(\mathbf{x}_1, \mathbf{x}_2) = h_{\alpha\gamma}(|\mathbf{x}_1 - \mathbf{x}_2|)$, etc., thus recovering Eqs. (4), (6), and (10).

APPENDIX B: NUMERICAL SOLUTION

The iterative method employed here works as follows. In the basic cycle, we start with an initial set of functions $\xi_{ij}^s(r)$ from which the functions $c_{ij}^s(r)$ are obtained by using $c_{ij}^s(r) = h_{ij}(r) - \xi_{ij}^s(r)$, where $h_{ij}(r)$ is given by Eqs. (32) and (33). Next, these short-range direct correlation functions are Fourier transformed to generate the functions $\tilde{c}_{ij}^s(k)$ to be inserted into the relationship obtained from Eqs. (4) and (14)

$$\mathbf{H} = (\mathbf{I} - (\mathbf{C} - \ell_b \tilde{\upsilon}(k)\mathbf{Z}\mathbf{Z}^{\mathrm{T}})\mathbf{R})^{-1}$$
$$\times (\mathbf{C} - \ell_b \tilde{\upsilon}(k)\mathbf{Z}\mathbf{Z}^{\mathrm{T}}), \tag{B1}$$

where $\tilde{z}_i(k) = q_i$, yielding the functions $\tilde{h}_{ij}(k)$. Finally, the inverse Fourier transform of $\tilde{\xi}_{ij}^s(k) = \tilde{h}_{ij}(k) - \tilde{c}_{ij}^s(k)$ provides a new set of functions $\xi_{ij}^s(r)$ to be used as the initial set for the next cycle. The function $b_{ij}^{\mathrm{ext}}(r)$ appearing in Eq. (33) can be initially set to zero, and subsequently be extrapolated from the $b_{ij}(r)$ determined for $r \leq R_{ij}^c$. This can be done by using a

specific functional form like $(A_{ij} + B_{ij}\cos(\omega_{ij}r) + C_{ij}\sin(\omega_{ij}r))\exp(-\lambda_{ij}r)/r$, or by a relationship involving the short-range indirect correlation functions like $\sum_p a_{ijp}\,\xi_{ip}^s(r)\,\xi_{pj}^s(r)$, etc. One can compare results from different approximations to estimate the accuracy of the calculations. However, as mentioned above, the contributions from these extrapolated bridge functions should be negligible when the cutoff distance is chosen large enough.

The Ng algorithm[77] uses the results from a few basic cycles to provide a better estimate of the $\xi_{ij}^s(r)$, usually improving the convergence of the method just described. Another useful trick is to multiply the parameter ℓ_b and the functions $h_{ij}(r)$ determined from Eqs. (32) and (33) by a factor x, which is then varied from 0 to 1. When $x = 0$ the exact solution is given by $\xi_{ij}^s(r) = 0$, and from this starting point the desired result is attained by incremental steps on x. On the other hand, if the simulation data are too noisy, it may be helpful to smooth the corresponding $h_{ij}^{\text{sim}}(r)$ by using sectional least-square fitting.

[1]*Dynamic Light Scattering: Applications of Photon Correlation Spectroscopy*, edited by R. Pecora (Plenum, New York, 1985).

[2]R. Krause, G. Nägele, D. Karrer, J. Scheneider, R. Klein, and R. Weber, Physica A **153**, 400 (1988).

[3]W. van Megen, S. M. Underwood, and P. N. Pusey, Phys. Rev. Lett. **67**, 1586 (1991).

[4]M. Quesada-Pérez, J. Callejas-Fernández, and R. Hidalgo-Álvarez, Adv. Colloid Interface Sci. **95**, 295 (2002).

[5]L. F. Rojas-Ochoa, R. Castañeda-Priego, V. Lobaskin, A. Stradner, F. Scheffold, and P. Schurtenberger, Phys. Rev. Lett. **100**, 178304 (2008).

[6]C. Haro-Pérez, L. F. Rojas-Ochoa, R. Castañeda-Priego, M. Quesada-Pérez, J. Callejas-Fernández, R. Hidalgo-Álvarez, and V. Trappe, Phys. Rev. Lett. **102**, 018301 (2009).

[7]M. Peláez-Fernández, A. Moncho-Jordá, and J. Callejas-Fernández, Europhys. Lett. **90**, 46005 (2010).

[8]J. C. Crocker and D. G. Grier, Phys. Rev. Lett. **73**, 352 (1994).

[9]M. D. Carbajal-Tinoco, F. Castro-Román, and J. L. Arauz-Lara, Phys. Rev. E **53**, 3745 (1996).

[10]J. C. Crocker and D. G. Grier, Phys. Rev. Lett. **77**, 1897 (1996).

[11]Y. Han and D. G. Grier, Phys. Rev. Lett. **91**, 038302 (2003).

[12]M. Polin, D. G. Grier, and Y. Han, Phys. Rev. E **76**, 041406 (2007).

[13]C. Gutsche, U. F. Keyser, K. Kegler, F. Kremer, and P. Linse, Phys. Rev. E **76**, 031403 (2007).

[14]M. D. Carbajal-Tinoco, R. Lopez-Fernandez, and J. L. Arauz-Lara, Phys. Rev. Lett. **99**, 138303 (2007).

[15]B. V. R. Tata, P. S. Mohanty, and M. C. Valsakumar, Solid State Commun. **147**, 360 (2008).

[16]E. W. Gomez, N. G. Clack, H.-J. Wu, and J. T. Groves, Soft Matter **5**, 1931 (2009).

[17]P. Tan, J. Huang, D. Liu, W. Tian, and L. Zhou, Soft Matter **6**, 4800 (2010).

[18]E. J. W. Verwey and J. Th. G. Overbeek, *Theory of the Stability of Lyophobic Colloids* (Elsevier, New York, 1948).

[19]W. B. Russel, D. A. Saville, and W. R. Schowalter, *Colloidal Dispersions* (Cambridge University Press, Cambridge, 1989).

[20]M. Medina-Noyola and D. A. McQuarrie, J. Chem. Phys. **73**, 6279 (1980).

[21]G. M. Bell, S. Levine, and L. N. McCartney, J. Colloid Interface Sci. **33**, 335 (1970).

[22]G. N. Patey, J. Chem. Phys. **72**, 5763 (1980).

[23]S. Alexander, P. M. Chaikin, P. Grant, J. Morales, P. Pincus, and D. Hone, J. Chem. Phys. **80**, 5776 (1984).

[24]L. Belloni, M. Drifford, and P. Turq, Chem. Phys. **83**, 147 (1984).

[25]B. Beresford-Smith, D. Y. C. Chan, and D. J. Mitchell, J. Colloid Interface Sci. **105**, 216 (1985).

[26]L. Belloni, J. Chem. Phys. **85**, 519 (1986).

[27]S. Khan, T. L. Morton, and D. Ronis, Phys. Rev. A **35**, 4295 (1987).

[28]H. Ruíz-Estrada, M. Medina-Noyola, and G. Nägele, Physica A **168**, 919 (1990).

[29]H. Löwen and G. Kramposthuber, Europhys. Lett. **23**, 673 (1993).

[30]O. Spalla and L. Belloni, Phys. Rev. Lett. **74**, 2515 (1995).

[31]L. Belloni and O. Spalla, J. Chem. Phys. **107**, 465 (1997).

[32]R. van Roij and J.-P. Hansen, Phys. Rev. Lett. **79**, 3082 (1997).

[33]L. Belloni, Colloids Surf., A **140**, 227 (1998).

[34]E. Allahyarov, H. Löwen, and S. Trigger, Phys. Rev. E **57**, 5818 (1998).

[35]E. Allahyarov, I. D'Amico, and H. Löwen, Phys. Rev. Lett. **81**, 1334 (1998).

[36]P. González-Mozuelos and M. D. Carbajal-Tinoco, J. Chem. Phys. **109**, 11074 (1998).

[37]J. Z. Wu, D. Bratko, H. W. Blanch, and J. M. Prausnitz, J. Chem. Phys. **111**, 7084 (1999).

[38]L. Belloni, J. Phys.: Condens. Matter **12**, R549 (2000).

[39]P. Linse and V. Lobaskin, J. Chem. Phys. **112**, 3917 (2000).

[40]J.-P. Hansen and H. Löwen, Annu. Rev. Phys. Chem. **51**, 209 (2000).

[41]V. Lobaskin, A. Lyubartev, and P. Linse, Phys. Rev. E **63**, 020401 (2001).

[42]C. N. Likos, Phys. Rep. **348**, 267 (2001).

[43]M. D. Carbajal-Tinoco and P. González-Mozuelos, J. Chem. Phys. **117**, 2344 (2002).

[44]J. A. Anta and S. Lago, J. Chem. Phys. **116**, 10514 (2002).

[45]M. Aubouy, E. Trizac, and L. Bocquet, J. Phys. A **36**, 5835 (2003).

[46]E. Trizac, L. Bocquet, M. Aubouy, and H. H. von Grünberg, Langmuir **19**, 4027 (2003).

[47]A. R. Denton, Phys. Rev. E **70**, 031404 (2004).

[48]J. A. Anta, J. Phys.: Condens. Matter **17**, 7935 (2005).

[49]R. N. Behera and P. Gupta-Bhaya, J. Chem. Phys. **126**, 044908 (2007).

[50]E. Allahyarov and H. Löwen, J. Phys.: Condens. Matter **21**, 424117 (2009).

[51]T. E. Colla, Y. Levin, and E. Trizac, J. Chem. Phys. **131**, 074115 (2009).

[52]A. R. Denton, J. Phys.: Condens. Matter **22**, 364108 (2010).

[53]T. E. Colla and Y. Levin, J. Chem. Phys. **133**, 234105 (2010).

[54]G. I. Guerrero-García, P. González-Mozuelos, and M. Olvera de la Cruz, J. Chem. Phys. **135**, 164705 (2011).

[55]M. Turesson, B. Jönsson, and C. Labbez, Langmuir **28**, 4926 (2012).

[56]R. Kjellander and D. J. Mitchell, J. Chem. Phys. **101**, 603 (1994).

[57]R. Kjellander and D. J. Mitchell, Mol. Phys. **91**, 173 (1997).

[58]J. Ulander and R. Kjellander, J. Chem. Phys. **114**, 4893 (2001).

[59]T. Laaksonen, P. Ahonen, C. Johans, and K. Kontturi, ChemPhysChem **7**, 2143 (2006).

[60]Y. Marcus, Chem. Rev. **88**, 1475 (1988).

[61]R. A. Robinson and R. H. Stokes, *Electrolyte Solutions* (Dover, London, 1959).

[62]J. F. Coetzee and G. P. Cunningham, J. Am. Chem. Soc. **87**, 2529 (1965).

[63]G. I. Guerrero-García, P. González-Mozuelos, and M. Olvera de la Cruz, "Large counterions boost the solubility and renormalized charge of suspended nanoparticles" (unpublished).

[64]S. Plimpton, J. Comput. Phys. **117**, 1 (1995).

[65]*LAMMPS Molecular Dynamics Simulator*, see http://lammps.sandia.gov/ (August 20, 2010).

[66]S. Nosé, Mol. Phys. **52**, 255 (1984).

[67]W. G. Hoover, Phys. Rev. A **31**, 1695 (1985).

[68]G. I. Guerrero-García, E. González-Tovar, and M. Olvera de la Cruz, Soft Matter **6**, 2056 (2010).

[69]B. A. Grzybowski, B. Kowalczyk, I. Lagzi, D. Wang, K. V. Tretiakov, and D. A. Walker, Faraday Discuss. **159**, 201 (2012).

[70]Z.-Y. Wang and Y. Q. Ma, J. Phys. Chem. B **114**, 13386 (2010).

[71]B. Modak, C. N. Patra, S. K. Ghosh, and P. Das, J. Phys. Chem. B **115**, 12126 (2011).

[72]L. Lue and P. Linse, J. Chem. Phys. **135**, 224508 (2011).

[73]P. X. Viveros-Méndez and A. Gil-Villegas, J. Chem. Phys. **136**, 154507 (2012).

[74]J. Wen, S. Zhou, Z. Xu, and B. Li, Phys. Rev. E **85**, 041406 (2012).

[75]F.-H. Wang, Y.-Y. Wu, and Z.-J. Tan, Biopolymers **99**, 370 (2013).

[76]Z. Xu, Phys. Rev. E **87**, 013307 (2013).

[77]K. Ch. Ng, J. Chem. Phys. **61**, 2680 (1974).